

# Colloidal black gold with broadband absorption for plasmon-induced dimerization of 4-nitrothiophenol and cross-linking of thiolated diazonium compound

Radwan M. Sarhan,<sup>a,c</sup> Sergio Kogikoski Jr.,<sup>b\*</sup> Robin M. Schürmann,<sup>b</sup> Yuhang Zhao,<sup>a</sup> Andreas Krause,<sup>b</sup> Bernd Schmidt,<sup>b</sup> Ilko Bald,<sup>b</sup> and Yan Lu<sup>a,b\*</sup>

<sup>a</sup> Department for Electrochemical Energy Storage, Helmholtz Zentrum Berlin für Materialien und Energie, Hahn-Meitner-Platz 1, 14109 Berlin, Germany

<sup>b</sup> Institute of Chemistry, University of Potsdam, 14467 Potsdam, Germany

<sup>c</sup> Chemistry Department, Faculty of Science, Cairo University, 12613 Cairo, Egypt

\*Correspondence: [kogikoski junior@uni-potsdam.de](mailto:kogikoski junior@uni-potsdam.de); [yan.lu@helmholtz-berlin.de](mailto:yan.lu@helmholtz-berlin.de)

## Abstract

Broadband light absorbers are very attractive for many applications, including solar energy conversion, photothermal therapy, and plasmonic nanocatalysis. Black gold nanoparticles are an excellent example of broadband light absorbers in the visible and near-infrared (NIR) ranges; however, their synthesis typically requires multi-step deposition or high temperatures. Herein, we report the synthesis of black gold via a facile, one-step green method using commonly known precursors (chloroauric acid and sodium citrate) performed at room temperature. The formation of the black gold particles is driven by the self-assembly of in-situ formed small nanoparticles (~ 5 nm) followed by a fusion step creating extensive networks of nanowires. These assemblies include intense hotspots for enhancing the electric field and the local temperature. Thus, the nanowires exhibit a strong photothermal effect and SERS performance. The plasmonic reactivity of the black gold is first tested using the dimerization reaction of 4-nitro thiophenol. In addition, we used the strong SERS signal enhancement to monitor the kinetics of plasmon-induced cross-linking of designed thiolated benzene diazonium molecules. Analysis of the reaction performed with external heating in the dark and under light irradiation confirmed the dominant mechanism of the charge transfer effect (i.e., hot electrons). Our work offers a new possibility to design efficient light-absorbing materials to achieve good solar-to-chemical/thermal energy conversion.

**Keywords:** black gold, hot electrons, plasmonic chemistry, SERS.

## Introduction

Sunlight is the most abundant energy source on earth. However, to use this energy, photons must be captured first. Thanks to their surface plasmon properties, noble metals with nanoscopic dimensions (nanostructures) strongly interact with and harvest the incident light.<sup>1-3</sup> As a result, energetic charge carriers (hot electrons and holes) and a high local temperature are generated, offering new perspectives of light-driven chemistry, known as plasmonic chemistry.<sup>4,5</sup> Plasmonic nanocatalysis was shown to initiate novel reaction pathways described either via the generation of hot charge carriers or by a thermally-induced mechanism.<sup>6-9</sup> The dimerization of 4-nitro thiophenol and 4-amino thiophenol have been considered the first examples of plasmonic chemistry, followed by other reactions driven by plasmonic effects.<sup>10-15</sup>

Plasmonic nanostructures made from gold, silver, and copper nanoparticles exhibit strong absorption in the visible and near-infrared range of the solar spectrum, unlike the traditional semiconductors that catalyze chemical reactions only with the highly energetic UV light.<sup>16-18</sup> Importantly, plasmonic nanoparticles' optical properties largely depend on their shape and size, which can be effectively tuned to capture specific photon energies. However, light harvesting by individual plasmonic particles is limited to a narrow spectral range that resonates with the plasmon frequency. In contrast, black gold superstructures made of assemblies of plasmonic nanoparticles exhibit a strong absorption over a broadband of the solar spectrum owing to their interparticle plasmonic coupling.<sup>19-22</sup> The fabrication methods, however, require multiple assembly steps or high temperatures. Several successful black gold synthesis attempts have been reported in the past few years. For instance, plasmonic colloidosomes of black gold have been prepared by a nucleation–growth synthetic approach.<sup>23</sup> In this approach, small gold nanoparticles were deposited on dendritic fibrous nanosilica, while the interparticle distances were controlled via a cycle-by-cycle growth approach of the gold particles. A direct one-step method at high temperatures was developed to achieve colloidal black gold superstructures.<sup>24</sup> This method is based on assembling in-situ formed nanoparticles owing to their solvophobic interaction with the solvent. Lately, an overcurrent electrodeposition method was also used to fabricate a fractal plasmonic black gold directly on a conductive surface.<sup>25</sup> However, it remains a significant

challenge to develop a simple one-step method for fabricating a colloidal plasmonic black gold nanostructure without requiring high temperatures or post-synthesis assembly steps.

Herein, we report the synthesis of black gold nanoparticles via a facile, one-step green approach, resembling the traditional Turkevich synthesis. This approach is based on simply mixing the gold precursor salt and sodium citrate at room temperature at a basic pH. The black gold nanostructures are formed due to the assembly of in-situ-formed small gold nanospheres, forming nanowires. Such morphology provides SERS substrates with intense hot spots to efficiently generate hot charge carriers for performing chemical transformation of surface-bound 4-nitro thiophenol (4-NTP) and diazonium molecules monitored by Raman spectroscopy. First, the plasmonic reactivity of the black gold is shown by using the dimerization reaction of 4-NTP into dimercaptoazobenzene (DMAB) as a typical model reaction. Second, we confirm that the hot electrons can also initiate cross-coupling of the adsorbed diazonium salt. The Raman spectra showed that the diazonium molecules are self-assembled in a dimer form, resembling the typical DMAB structures.<sup>26</sup> Second, upon continuous excitation of the surface plasmon, the Raman peak assigned to the N=N vibrational modes decreases in intensity. In contrast, the C=C peak is broadened with time, suggesting the cross-linking of the adsorbed molecules accompanied by nitrogen removal. Additionally, by comparing the reaction behavior performed with external heating in the dark and under irradiation, we show that the hot electrons play the dominant role in initiating the reaction.

## Experimental section

**Chemicals.** Chloroauric acid trihydrate ( $\text{HAuCl}_4 \cdot 3\text{H}_2\text{O}$ ), sodium hydroxide (NaOH), sodium citrate tribasic hydrate, N-(2-Hydroxyethyl)piperazine-N'-(2-ethanesulfonic acid) (HEPES), Silver nitrate (99%), and glycerol were purchased from Aldrich. 4-mercapto-benzenediazonium tetrafluoroborate was synthesized according to the previous protocol.<sup>27</sup> All the chemicals were used without further purification.

**Synthesis of black gold nanowires.** The particles were prepared in a one-step synthesis at room temperature. Briefly, 1 ml of 25 mM of an aqueous chloroauric acid solution was placed in a glass

vial, and the pH was first adjusted by adding 150  $\mu\text{L}$  of 0.5 M NaOH. Finally, different volumes of 1% aqueous sodium citrate solution ( $\text{Na}_3\text{Cit}$ , 250, 700, and 1000  $\mu\text{L}$ ) were added and mixed for 5 minutes. The solution was left undisturbed for 1 hour till the color changed from yellow to gray and finally dark black, confirming the reduction process. The gold particles were washed with deionized water and separated by centrifugation (6000 rpm, 12 min). The nanowires were then dispersed in water for further use. To compare the plasmonic activity towards the cross-linking of the diazonium molecules, gold nanoparticles known as gold nanoflowers (AuNFs) and silver nanoparticles (AgNPs) have been prepared according to our recent published protocols and used as plasmonic substrates for the reaction.<sup>11,28</sup>

**SERS substrate.** Before the Raman measurements, the silicon substrate was cleaned in a solution of 30 wt %  $\text{H}_2\text{O}_2$  and 30 wt %  $\text{H}_2\text{SO}_4$ . The substrate was then washed with deionized water and ethanol. Afterward, 50  $\mu\text{l}$  of the gold solution was placed on the cleaned substrate and dried before use. The gold nanowires assembled on the substrate were immersed in either 1 mM of 4NTP or 1 mM of  $\text{N}_2\text{TP}^+\text{BF}_4^-$  for 1 h, both molecules were solubilized in ethanol. The sample was washed with ethanol to remove the loosely bound molecules and dried before being measured.

**Photothermal conversion performance.** The photothermal conversion performance of the gold nanowires was examined using an aqueous dispersion of the particles. Briefly, 0.5 ml of the gold nanowires dispersion was added to an equal volume of deionized water in a standard 1-cm thick quartz cuvette with a final concentration of ca. 0.1  $\text{mg mL}^{-1}$ . The sample was irradiated via an 808-nm NIR laser (PhotonTec Berlin, turn-key 808 nm diode laser system) with different laser powers (2.0-4.0  $\text{W cm}^{-2}$ ) for more than 10 minutes. The temperature increments of the dispersions were directly recorded by a digital thermometer (P300 Thermometer, Dostmann electronics) at each time interval, the thermometer was kept far away from the laser spot to avoid its direct heating by light.

**Methods.** Transmission electron microscopy (TEM) examined the nanoparticles' morphology using a JEOL JEM-2100 (JEOL GmbH, Eching, Germany) at an acceleration voltage of 200 kV. The samples were prepared by placing a drop of the diluted nanoparticles solution on the carbon-coated copper grids and left to dry under ambient conditions. UV-vis-NIR spectra were recorded

using a Lambda 650 spectrophotometer supplied by PerkinElmer. SERS spectra have been recorded using a confocal Raman microscope (WITec 300α) equipped with an upright optical microscope. For Raman excitation, laser light at  $\lambda = 488, 532, 633,$  and  $785$  nm was coupled into a single-mode optical fiber and focused through a 50× objective (Olympus MPlanFL N, NA = 0.75) to a spot size of about 1000 nm. The laser power was kept at 1 mW at the focal plane for all wavelengths, and the integration time was set to 1s. The kinetics were followed between 5 to 10 minutes for each sample, *i.e.*, each curve is based on 300 to 600 different spectra. Each sample was measured at least three times. To check the behavior of the modified substrate with temperature, a micro temperature controller with an extended temperature range substrate (VAHEAT, Interherence GmbH) was used. The black gold films were deposited over the heating element, and the temperature was varied from room temperature to 122 °C. The Raman spectra were measured with low-intensity laser incidence (100 μW) to induce the reaction by temperature and not by light irradiation. A long working distance of 50× objective was used to avoid contamination of the objective lens with possible volatile compounds emitted by the sample.

## **Results and discussion**

### **1. Material synthesis and characterization**

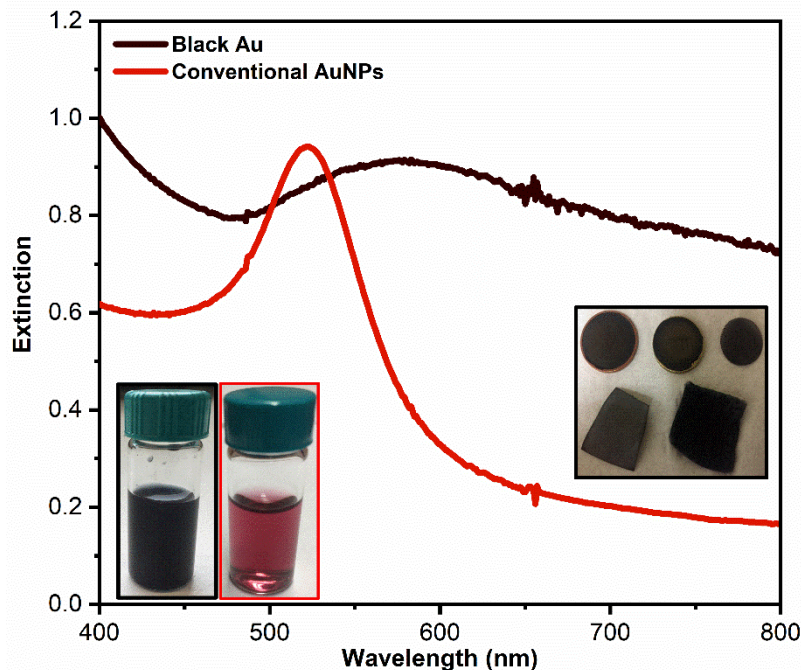


**Figure 1.** UV-vis spectrum of the black gold (black spectrum) and the conventional gold nanoparticles (red spectrum), the color of their corresponding solutions, and digital pictures of different substrates coated with black gold.

One-step fabrication of black gold nanoparticles is presented using sodium citrate as a reducing and capping agent, resembling the standard Turkevich synthesis. Unlike the Turkevich approach, the gold nanoparticles here were synthesized at room temperature, which slows down the reaction rate and, therefore, the nanoparticle nucleation and growth rate. Moreover, the gold nanoparticles synthesized at the boiling temperature are often characterized by the appearance of a wine-red color within 30 minutes and a narrow plasmon peak centered around 520 nm (Figure 1).<sup>29,30</sup> Herein, at room temperature, a black colloidal solution is gradually observed within 60 minutes with a broadband absorption all over the visible range (400–800 nm) as shown in Figure 1 as well as a part of the near-infrared region (not shown). The black gold can also transform reflective surfaces (e.g., 5- and 10-cent coins and copper mesh) and flexible surfaces (e.g., filtration paper and cotton substrate) into black absorbing surfaces by a simple drop-casting method (insets of Figure 1). Broadening the absorption band of black gold is very important for several applications where optical excitation with multiple photons is essential. For instance, in

ultrafast spectroscopy, such as the surface-enhanced coherent anti-Stokes Raman scattering, multiple laser pulses with different wavelengths should coincide with the absorption band of the gold nanoparticles.<sup>31</sup> Additionally, the resonance between the plasmon band and the excitation wavelength affects the reaction yield and rate in plasmonic catalysis, which can be easily tuned by broadening the plasmon band.<sup>32,33</sup> Thus, it presents a plasmonic black colloidal gold with a broadband absorption that works efficiently for many purposes. Briefly, different volumes of the sodium citrate ( $\text{Na}_3\text{Cit}$ ) were thoroughly mixed with the gold precursor ( $\text{Au}^{+3}$ ) at room temperature in the presence of sodium hydroxide. The solution was left undisturbed to allow the assembly and formation of the nanoparticles. The color of the solution changes from yellow to pale gray within 30 minutes and rapidly into dark black. TEM first examined the morphology of the as-prepared particles. As shown, the concentration of  $\text{Na}_3\text{Cit}$  has a significant effect on the morphology of the obtained particles. Figure 2a–d shows the formation of an extensive network of gold nanowires obtained using an  $\text{Au}^{+3}/\text{Na}_3\text{Cit}$  molar ratio of 1/1. The diameter of the individual nanowire is approximately 5 nm. The HRTEM image in Figure 2c shows the lattice spacing of 0.23 nm, which corresponds to the  $\langle 111 \rangle$  lattice plane of gold. Additionally, using different volumes of the  $\text{Na}_3\text{Cit}$  did not influence the black color of the colloidal solution. However, the morphology of the particles is affected. When we decreased the amount of the  $\text{Na}_3\text{Cit}$  (i.e., a molar ratio of 1/0.34), the gold nanowires can still be observed but with a high degree of clustering and irregular shapes, as shown in Figure S1a. The lower concentration of  $\text{Na}_3\text{Cit}$  and its lower passivation effect might be the reason for this clustering. On the other hand, when a higher amount of  $\text{Na}_3\text{Cit}$  is used (a molar ratio of 1/1.36), spherical gold particles and short gold chains have been observed (Figure S1b) since the assembly and the fusion of the initial gold nuclei are somehow deferred. In the absence of  $\text{NaOH}$ , only brown gold was observed, which is quickly agglomerated in the form of a sponge gold precipitate.

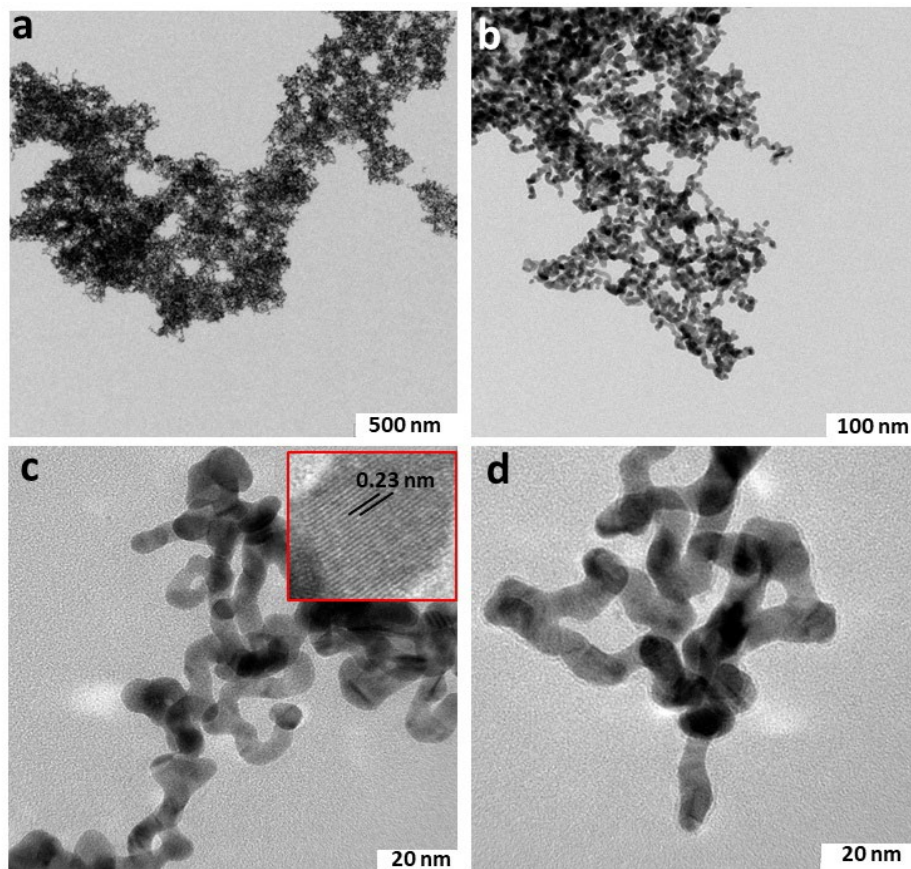


**Figure 2.** TEM images of the gold nanowires were prepared by adding 700  $\mu\text{L}$  sodium citrate to the gold precursor.

Observing spherical particles when the capping agent's concentration changes might hint at the mechanism of the nanowire's synthesis. This means that small spheroidal particles are formed, which assemble and fuse to form the nanowires. Therefore, using a high concentration of the  $\text{Na}_3\text{Cit}$  retards the fusion of these spheres, and only short chains and spherical particles, can be observed. To verify this mechanism, the intermediate product of the synthesis was collected after 30 minutes when the color of the suspension started to change (gray) and examined by TEM. It is worth noting that the sample was first diluted to retard the growth of the particles before being dried on the copper grid. However, the growth still proceeds slowly, and thus, different products can be observed, showing the various stages of the synthesis mechanism. As proposed, small spherical nanoparticles with a diameter of 5 nm have been observed and can be identified as the initial stage. These small in-situ formed spheres assemble and fuse to form rod-like

structures. The growth continues laterally to form the nanowires, as shown in Figures 3a and b. Additionally, Figure 3c shows a TEM image of a free nanowire that still preserves the spheres' shape, confirming our proposed mechanism. Finally, the gold nanowires are further interlaced, forming network-like structures and nanobundles, as illustrated in Figure 3d. Previously, Feng and co-workers have shown a similar growth mechanism. They synthesized ultrathin gold nanowires using the triisopropylsilane as a reducing agent and oleylamine as a stabilizer and a growth template. The authors observed small spherical nanoparticles (3-8 nm) as the initial stage.<sup>34</sup> The fusion of these nanoparticles led to the formation of chain-like nanoparticles, which were then transformed into smooth gold nanowires. In contrast, Polte and co-workers have investigated the growth mechanism underlying the classical Turkevich method, showing that the mechanism is mainly based on the coalescence and the growth of small gold nuclei ( $\sim 2 - 5.5$  nm) into bigger spherical particles.<sup>35</sup> Benefitting from the very broad plasmon band, we next discuss the two significant properties of plasmonic particles: the conversion of light into thermal energy and the use of visible light to induce chemical reactions.

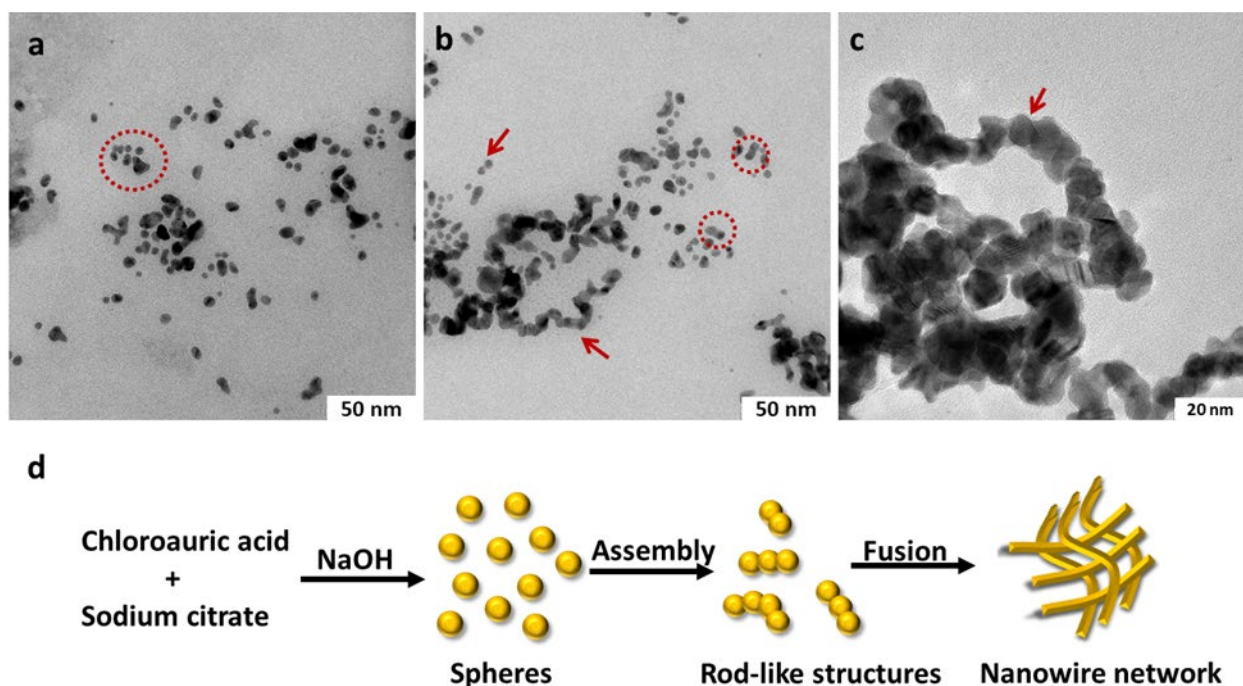


**Figure 3.** TEM images of the gold nanowires were taken after 30 minutes of the synthesis, showing their growth mechanism (a, b, and c) and corresponding schematic illustration (d).

## 2. Photothermal conversion performance

Plasmonic metal nanoparticles (e.g., Ag, Au) have been extensively used as nanoantenna for enhancing light scattering in many applications, such as surface-enhanced Raman scattering and optical imaging, owing to their large optical cross-sections as compared to organic dyes. Additionally, non-radiative decay of the surface plasmon would result in a significant temperature increase, which is highly localized on the nanoparticle.<sup>36</sup> Briefly, the optical excitation of plasmonic nanoparticles results in a coherent collective oscillation of the conduction-band electrons known as the localized surface plasmon (LSP). After light excitation, the decay of the excited LSP eventually results in a hot electron distribution within tens of femtoseconds. The hot electrons are often utilized in catalysis, as they can scatter to occupy the empty orbitals of the adsorbed molecules (i.e., reactants). Next, the hot electrons are scattered by the phonons, and their energy is transferred to the metal lattice, which increases the particle temperature (i.e., thermoplasmonic effect). The photothermal effect is finally observed as the thermal energy dissipates to the surrounding medium (i.e., ligand or solution). The thermoplasmonic effect of the black gold in the absence of any electron acceptors is here used as an indication for the robust harvesting of light and generation of hot electrons. Herein, the photothermal conversion effect of the black gold solution was examined while the particles were irradiated with NIR lasers (808 and 976 nm). Figure 4a shows the setup adopted to measure the photoheating effect. The nanoparticle dispersion is placed in a quartz cuvette and directly irradiated with different lasers. Meanwhile, the temperature of the solutions is simultaneously recorded every 20 seconds by a digital thermometer. Figure 4b shows the stepwise temperature increments of the particle suspensions under continuous light irradiation (808 nm). As shown, the temperature of the gold solution rises quickly with increasing light exposure time and reaches a steady state after 10 minutes. Using a laser intensity of  $3 \text{ W cm}^{-2}$ , the temperature of the black gold solution reaches a temperature of  $\sim 38^\circ\text{C}$ . The pure water showed a negligible temperature change ( $\sim 3.1 \text{ K}$ ) under the same laser intensity, clearly showing the direct photoheating effect of the black gold. The photothermal effect is modulated by changing the laser intensity, where the higher laser intensity tends to display a higher temperature increment. Indeed, the temperature increased to  $\sim 47^\circ\text{C}$  when the laser intensity was increased to  $4 \text{ Wcm}^{-2}$ . Moreover, by following

the method developed by Roper et al.,<sup>37</sup> we measured the black gold dispersion's photothermal transduction efficiency ( $\eta$ ) by monitoring the system's heat dissipation rate as the light source is shut off (Figure S2).<sup>38,39</sup> The particles showed a photothermal efficiency of 15.2 % under 808 nm irradiation, as shown in the supporting information. This is relatively higher than the gold nanospheres (20 nm,  $\eta = 7.68$  %) and urchin-like gold nanoparticles (120 nm,  $\eta = 11$ ) measured at the same excitation wavelength and power. However, we believe that the photothermal efficiency of the black gold would increase upon more resonant excitation (e.g., at 600 nm). In addition, the particles are still active photothermal nanoconverters when irradiated with a longer excitation wavelength (976 nm, Figure 4c) under the same experimental conditions due to their broad extinction spectrum. The temperature increment was 18.3 K, lower than the increment obtained using the 808 nm laser (23.1 K) at the same light intensity due to the different plasmon resonance conditions. The photostability of the gold solution is further examined by repeating the on/off cycle of the NIR laser irradiation. As shown in Figure 4d, the photothermal efficiency of the black gold displays a stable reversible temperature response for three on/off cycles without a significant loss of the heating capacity. The black gold has been proven to be a robust NIR-responsive nano-heater capable of harvesting and converting light into heat.

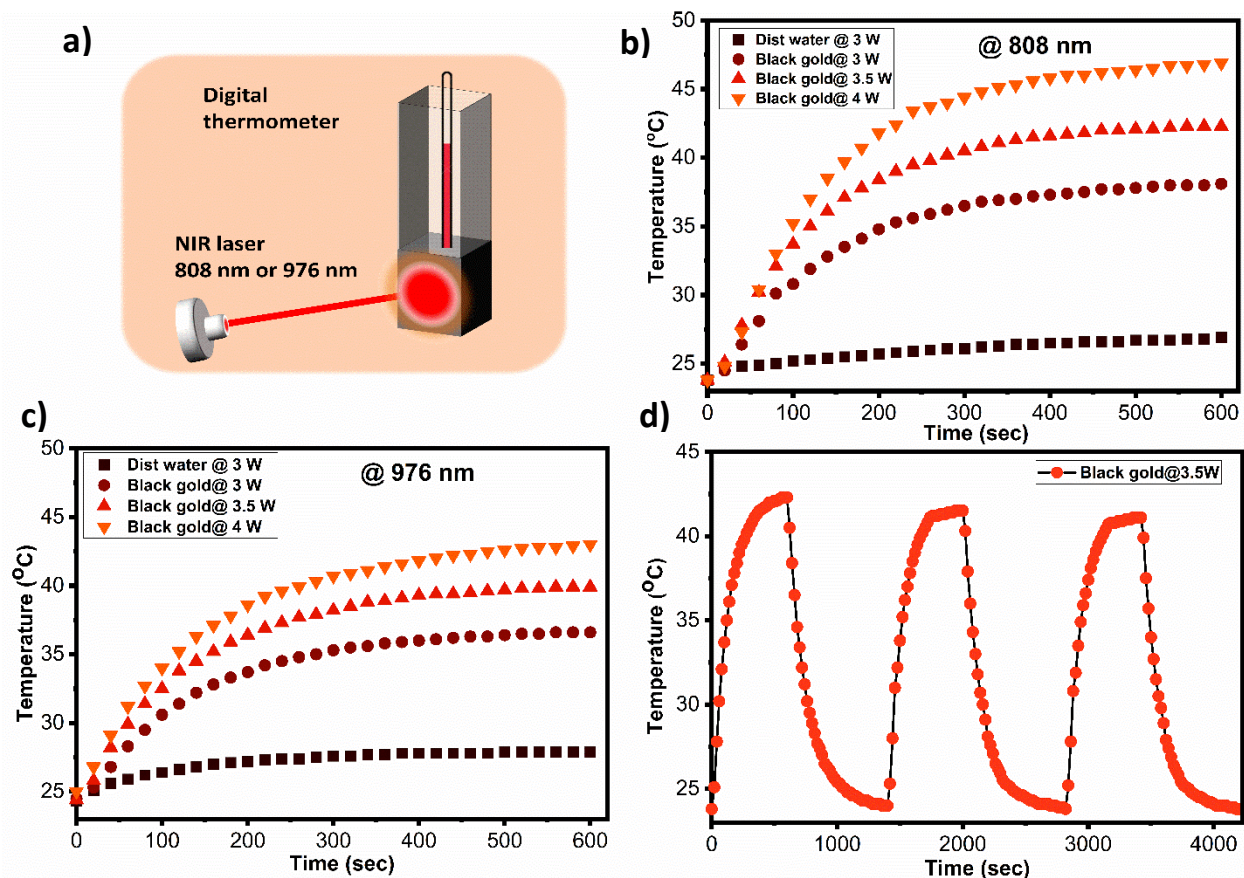


**Figure 4.** (a) Schematic presentation of the setup adopted for measuring the photothermal effect of the gold, (b) temperature variation curves of the aqueous dispersions of black gold exposed to the 808 nm laser at different laser powers, (c) temperature variation curves of the aqueous dispersions of black gold exposed to the 976nm laser at different laser powers, (d) photostability of the black gold solution under the photothermal heating conditions (808 nm, 3.5 W/cm<sup>2</sup>) and natural cooling cycles.

### 3. Dimerization of 4-nitrothiophenol

Hot charge carriers (hot electron/hole pairs) generated by the non-radiative relaxation of the surface plasmon can also induce chemical changes in the adsorbed molecules. Various chemical reactions have been recently shown to be driven or enhanced, benefitting from plasmon excitation, including N-N and C-C coupling reactions and reduction and desorption reactions.<sup>36–</sup>

<sup>38</sup> Additionally, a strong local electromagnetic field is generated in the near field close to the particle surface, owing to the localization of light around these small nanoparticles. This strong

electric field is often utilized to amplify the weak Raman scattering as the primary contributor to surface-enhanced Raman scattering (SERS). This enhancement is particularly strong in “hot spot” areas, e.g., in nano-sized gaps between the plasmonic particles or at nanotips with high aspect ratios.

Herein we first perform SERS analysis to unfold the capability of the black gold to induce catalytic reactions on their surfaces. The dimerization of 4-nitro thiophenol (4-NTP) into dimercaptoazobenzene (DMAB) is, therefore, used as a model reaction, as this reaction has been commonly explained by the effect of the charge-transfer (i.e., hot electrons), Figure 5a. The particles were drop cast onto a clean silicon substrate, followed by the self-assembly of the 4-nitro thiophenol molecules through the Au-S covalent bond. As shown in Figure 5b, the initial SERS spectra are dominated by the three prominent Raman peaks of the 4-NTP observed at 1080, 1343, and 1573  $\text{cm}^{-1}$ , assigned to the C–H bending,  $\text{NO}_2$  symmetric stretching, and C=C stretching modes of 4-NTP, respectively.<sup>40</sup> Additionally, the high SERS signal enhancement of 4-NTP adsorbed on the black gold can be directly noticed in the spectra.

Moreover, as the laser power increased, three new Raman peaks were observed, as shown in Figure 5c. These new peaks at 1134, 1387, and 1434  $\text{cm}^{-1}$  are assigned to the C–N symmetric stretching and N=N stretching vibrational modes of plasmonic-generated DMAB,<sup>26</sup> implying the high plasmonic reactivity of the gold nanowires. In this way, the plasmonic black gold provides the adsorbed 4-NTP molecules with the hot electrons and as a SERS substrate to enhance the Raman scattering.<sup>11,13</sup> Different laser powers were tested to visualize further the catalytic activity and the dependency of the reaction with the incident laser power. Unfortunately, due to the extremely high photothermal efficiency of the black gold nanowires, the NTP and DMAB thermally desorbed from the surface of the nanoparticles, turning such analysis impossible, as observed in Figure 5d, where the whole spectra decrease over time, an indication that the molecules are desorbing from the nanoparticle surface. To overcome such obstacles, we used the molecule 4-mercapto-benzene-diazonium tetrafluoroborate (MBD), which generates a molecule with a similar fingerprint as a starting material to DMAB, and that is stable enough for desorption to be studied with many laser wavelengths.

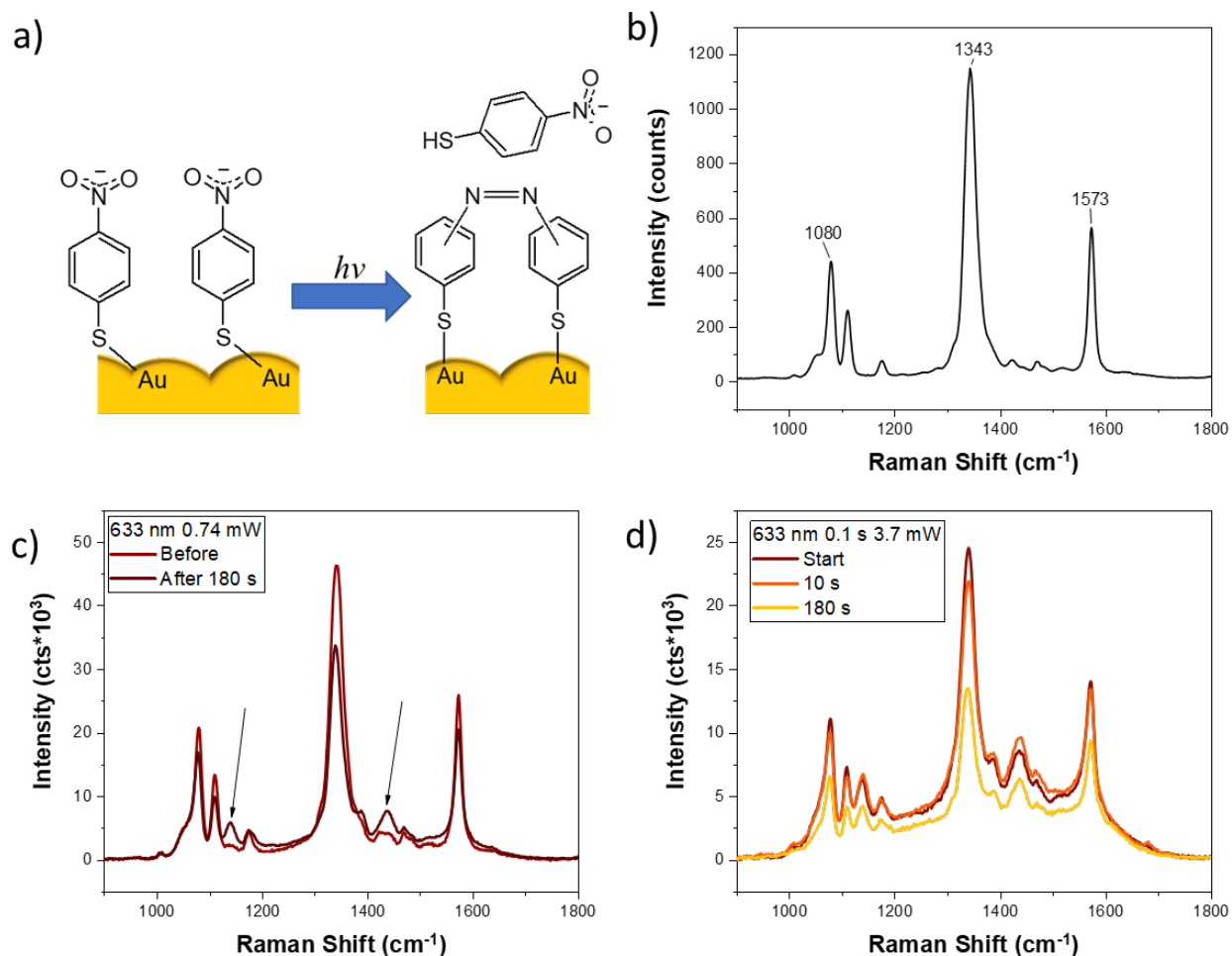


**Figure 5.** a) Scheme of the monitored reaction of the plasmonically induced dimerization of 4NTP to DMAB. B) SERS spectrum of 4-NTP assembled on the gold nanowires measured at a laser power of 0.14 mW, c) SERS spectra of the black gold nanowires at the beginning of the irradiation and after 180 s showing the appearance of the peaks associated with DMAB, laser power of 0.74 mW d) SERS spectrum obtained using 3.7 mW of laser power showing for the beginning a high amount of DMAB, which maximizes after 10 s and the overall spectrum decrease associate with the desorption of the molecules from the surface after 180 s of irradiation.

#### 4. Hot electron-induced cross-linking reaction

Next, we applied SERS to in-situ investigate the plasmon-induced reactivity of aryldiazonium compounds. They represent versatile building blocks in synthetic organic chemistry, including important cross-coupling reactions such as Suzuki and Heck reactions.<sup>41</sup> Importantly, we aim to showcase whether the hot electrons generated from the LSPR can induce chemical transformations of the diazonium salts adsorbed onto the metal nanoparticles. Surface functionalization of metal particles with aryldiazonium has been recently observed with the assistance of plasmon excitation. This provides a stable organic layer with a range of functional groups and enables the particles to be stably dispersed in different reaction media. One interesting case was reported by Nguyen Van Quynh and co-workers, where gold nanotriangles were grafted with an organic layer of diazonium salts induced by light irradiation.<sup>42</sup> The work shows that the grafting can be only achieved by using a proper light excitation, i.e., in resonance with the LSPR. More importantly, the grafting process is believed to be driven by hot electrons due to the generation of very localized products (at the tips of the nanotriangles), as observed by scanning electron microscopy, that could be used to visualize the electromagnetic fields around the particles experimentally. However, the mechanism and the sequential steps of the assembly and coupling of the diazonium-based compounds into such an organic layer still need to be determined.

To further investigate such a process, surface-enhanced Raman scattering (SERS) provides information on the vibrational fingerprints of the molecules upon their assembly and reaction. We used 4-mercapto-benzene-diazonium tetrafluoroborate (MBD) molecules as they can chemically adsorb on the gold surface by a covalent Au-S bond. The particles were drop cast onto a clean silicon substrate, followed by the self-assembly of the 4-mercapto-benzene-diazonium tetrafluoroborate (MBD) onto the particles' surfaces. This molecule was chemically designed to provide a possibility to attach through the thiol group to the surface of the gold by the Au-S covalent bond. Later, we could observe the  $N_2^+$  leaving due to the plasmonic reactivity.<sup>27</sup> Figure 6 shows the Raman signature of MBD adsorbed on the black gold compared to the neat molecules. As shown, due to the diazonium moiety, different surface attachment configurations are possible by both the Au-N and Au-C bonds. The typical Raman spectrum of the MBD molecule shows prominent peaks at  $1008\text{ cm}^{-1}$  (monosubstituted aromatic ring breathing mode),  $1069\text{ cm}^{-1}$

<sup>1</sup> (C-H in-plane bending of the aromatic ring), 1560 cm<sup>-1</sup> (C=C stretching and ring deformation), and at 2277 cm<sup>-1</sup> (N<sub>2</sub><sup>+</sup> stretching, not shown here).<sup>43</sup> When the molecules are deposited onto the Black gold films, we observe the appearance of new peaks and the shift of existing peaks due to their chemical adsorption onto the gold surface.

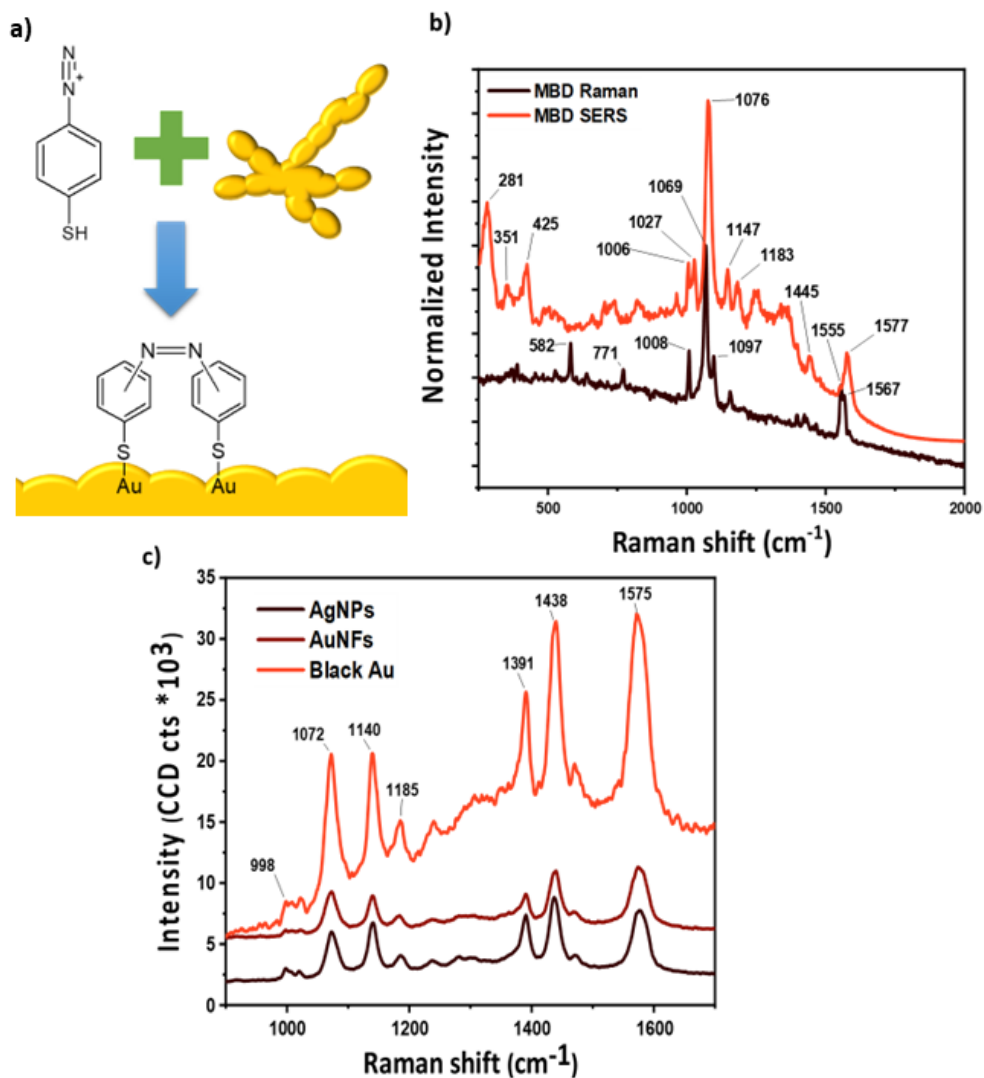


**Figure 6.** a) Scheme showing the adsorption of the MBD molecule over the Black Au surface. b) Raman and SERS spectra of the MBD molecule, using  $\lambda=785$  nm. c) Comparison of the SERS spectra obtained at  $\lambda=633$  nm for the films based on Black Au, AgNPs, and AuNFs.

The SERS spectra of the MBD adsorbed on the nanoparticles clearly show new bands not present in the normal Raman spectrum and the absence of other bands. The peaks at ~1140, 1185, 1395,

and  $1440\text{ cm}^{-1}$  are not related to the original MBD molecules but rather to an azobenzene derivative (Figure 6a and b), similar to the very common dimercaptoazobenzene (DMAB).<sup>11,26</sup> The peak for the  $\text{N}_2^+$  stretching around  $2200\text{ cm}^{-1}$  is not observed. Since the diazonium moiety is very reactive, the self-assembled MBD molecules may be sufficiently close to each other on the gold surface to react and dimerize.

The possibility of black Au being used in plasmonically induced reactions was tested using the MBD self-assembled monolayer and monitored by in-situ SERS measurements. Four different wavelengths were used, and the results were also compared to typical silver nanoparticles (AgNPs) and gold nanoflowers (AuNFs) aggregated similarly to black Au. Using 633 nm, the SERS spectra of the black gold exhibit 3.5 times higher peak intensities than AgNPs and AuNFs (Figure 6c). The reaction was initiated by continuously irradiating the samples for at least 300 seconds using a laser power of 1 mW in the focal point. The overall result is similar in all studied cases. As shown in Figure 7a, over time, there is a decrease in intensity of all the vibrational peaks and, at the same time, a broadening of the peak around  $1590\text{ cm}^{-1}$ . The loss of the diazonium moiety (C-N=N-C) is mainly observed by the intensity decrease of the peaks at  $1391$  and  $1438\text{ cm}^{-1}$ , associated with the diazonium vibrations. It is often expected that new peaks appear due to the formation of a reaction product, which is not the case here. However, these results suggest the dissociation of the N=N groups and coupling of the remaining benzene rings into a molecular carbonaceous layer, as evidenced later by the observation of amorphous carbon bands after prolonged irradiation (1.5 h). Recently, it was reported using tip-enhanced Raman spectroscopy (TERS) that due to the light irradiation of plasmonic nanoparticles, a broadening of the peaks in the spectrum is observed because of the formation of non-organized carbonaceous compounds, carbon nanomembranes, or amorphous carbon.<sup>44,45</sup> It was shown that such broadening is not due to a fully thermal reaction but that the hot electrons generated in the gold nanotips are the main driver of the reaction. At the same time, control experiments by heating the samples in the dark showed thermal-induced desorption of the molecules from the surface rather than their cross-linking.

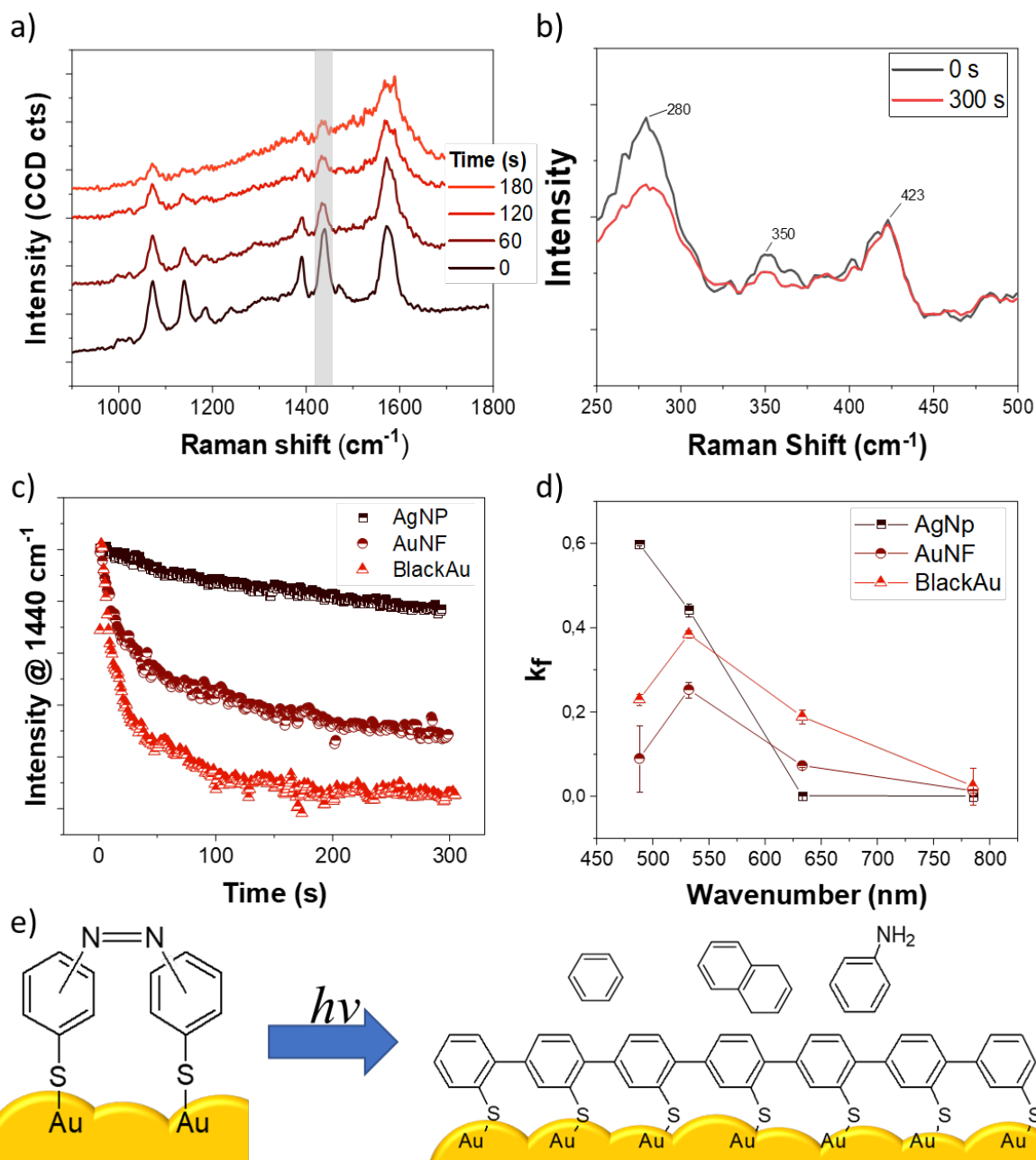


**Figure 7.** a) SERS spectra collected at the different irradiation times over black Au modified with MBD,  $\lambda=633$  nm and 1 mW of laser power at the focal point, 1 s of integration time. b) SERS spectra in the low-frequency region of the modified black Au films at 0 and after 300 s irradiation,  $\lambda=785$  nm and 1 mW of laser power at the focal point, 1 s of integration time. c) Intensity of the 1440  $\text{cm}^{-1}$  peak over time for the three studied materials,  $\lambda=633$  nm. d) Comparison of the fitted  $k_f$  with the different wavelengths tested in this work for the three studied materials. e) a

schematic presentation of the suggested chemical changes of the MBD induced by plasmonically generated hot electrons, leading to the partial evaporation of aromatic molecules and the formation of a carbon nanomembrane on top of the particles.

A similar reaction route is most likely followed in the present case, where MBD serves as a starting material. Due to the light irradiation, hot carriers are generated in the black gold nanoparticles leading to cross-linking reactions within the self-assembled molecules, which induce the peak broadening at  $1590\text{ cm}^{-1}$ . However, due to the excellent photothermal properties of black Au, the surface is also heated up very strongly, leading to the partial desorption of the molecules from the surface. This second part is better observed at the low-frequency vibrations, Figure 7b. By comparing the spectra at the beginning and after 300 s of irradiation, we observe that the peaks related to the Au-S lose intensity, indicating that those bonds are broken and some molecules possibly left the NP surface. At the same time, the very stable band at  $423\text{ cm}^{-1}$ , related to the Au-C or the C-S stretching of the thiol-linked molecule, kept the same intensity throughout the irradiation. Although we do not have a complete picture of the final material on the black Au NP surface, we hypothesize that the aromatic rings are linked together, forming a carbon nanomembrane on top of the black gold film, Figure 7e.

The wavelength dependence of the reaction is also investigated using four different wavelengths (488, 532, 633, and 785 nm) for all nanoparticles, as we plotted the intensity loss for the peak at  $1440\text{ cm}^{-1}$  over time (Figures 7c and d). We can now fit these curves using this data to obtain kinetic information about the reaction. We have recently shown that even though the kinetics curves obtained through SERS experiments carry little information about the reaction order, they are still very useful for comparing the different properties of the studied materials.<sup>46-48</sup> Here, we fitted the curves using a second-order fractal reaction kinetics equation:

$$[A] = \frac{[A]_0 * (1 - h)}{(1 - h) + [A]_0 * k_f * t^{1-h}}, \text{ (Equation 1)}$$

[A] is the intensity of the peak,  $[A]_0$  is the initial intensity,  $k_f$  is the fractal kinetics constant, t is time, and h is the fractal order. All the data studied here was fitted using this equation, and the overall fit quality is outstanding. The principal extracted value is  $k_f$ , which indicates the reaction's

speed. The plot of  $k_f v$  time (s) of the excitation wavelength for the three materials is given in Figure 7d. The results show that black Au exhibited an overall faster reaction than the AuNFs for all the studied wavelengths. In addition, the reaction exhibited a faster rate at 532 nm and a slowest rate at 785 nm. In contrast, AgNPs present faster kinetics at 488 nm. This is expected since the typical plasmonic resonance of the Au NPs, and AgNPs are located around 520 and 420 nm, respectively.<sup>49</sup> These results show the dependence of the reaction rate on the plasmon resonance of nanoparticles, which confirms the plasmonic nature of the cross-linking reaction of the assembled MBD molecules.

However, whether a charge transfer mechanism or the heating effect drives this behavior remains. To answer this question, we further performed a control experiment by adsorbing the nanostructures on a smart micro heating substrate (Interherence GmbH), allowing precise nanoparticle heating. We first reproduced our previous findings at room temperature while irradiating the sample continuously. As shown in Figure 8a, the two peaks at 1391 and 1438  $\text{cm}^{-1}$  completely vanished after 10 minutes, while the other SERS peaks were relatively stable. This confirms the formation of a carbon nanomembrane at the top of the black gold film.

Further irradiation (1.5 h) of the sample disturbs this layer and leads to the formation of an amorphous carbon layer, as evidenced by the appearance of the D-band at 1384  $\text{cm}^{-1}$ . For the comparison with the temperature-induced reaction, we conducted the reaction under heating in the dark, while the laser was only used to probe the reaction (less than 100  $\mu\text{W}$  of laser power at the focal point). As seen in Figure 8b, increasing the temperature from RT ( $\sim 22^\circ\text{C}$ ) to  $122^\circ\text{C}$  leads to the loss of SERS signals gradually, without observation of any distinct Raman bands. This behavior is commonly associated with the thermal-driven desorption/degradation of the adsorbed molecules.<sup>44,45</sup> At the same time, we observe that the initial vibration peaks are present throughout the study but lose intensity. Thus, these results confirm that the hot-electron transfer mechanism, Figure 8c, mainly drives the diazonium molecules' cross-linking reaction into a carbon nanomembrane. In contrast, the pure thermal mechanism (heating the sample in the dark) leads to desorption and degradation of the reactant molecules.

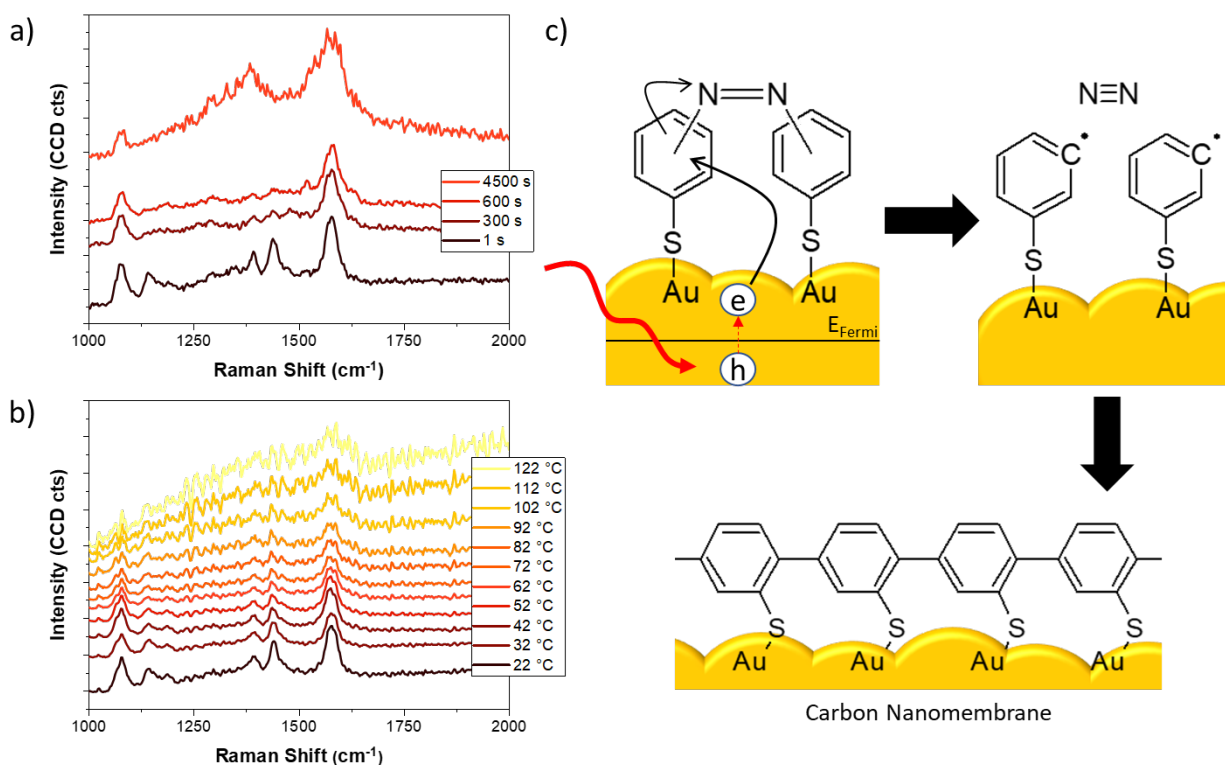


**Figure 8.** a) SERS spectra collected over Black Au modified with MBD performed at room temperature using a laser power of 1 mW at the focal point and integration time of 1 s. b) performed at different temperatures and probed using a laser power of 0.1 mW and integration time of 10 s. The wavelength used was  $\lambda = 633$  nm. c) Proposed reaction mechanism.

## Conclusion

In summary, we successfully developed a simple one-step synthesis of a plasmonic colloidal gold nanowire with broadband absorption in the visible and near-infrared ranges. The assembly and the fusion of small in-situ formed spherical particles ( $\sim 5$  nm) drove the growth mechanism. The gold particles displayed strong NIR photothermal as well as SERS performance. The SERS properties of the particles enabled us to monitor the plasmon-induced cross-linking of designed thiolated diazonium compounds adsorbed on the gold surface via the Au-S bond. The SERS spectra indicate the self-assembly of the molecules onto the gold surface in a dimer form via N=N coupling. At the same time, continuous irradiation led to cross-linking of the molecules and dissociation of N<sub>2</sub>. In general, this work provides a direct strategy to prepare black gold

nanostructures with broadband absorption that holds promising potential in many applications, including photothermal therapy, plasmon-driven-nanocatalysis, and photovoltaic cells.

### Supporting Information

TEM images of the black gold prepared using different concentrations of sodium citrate, measurement of photothermal efficiency, Fitting results of the kinetic study of the MNB decomposition, and SEM images of the black gold deposited on silicon wafer after heating at 122 °C.

### Acknowledgment

This research was supported by the European Research Council (ERC; consolidator grant no. 772752).

### References

- (1) Bi, Y.-G.; Feng, J.; Ji, J.-H.; Yi, F.-S.; Li, Y.-F.; Liu, Y.-F.; Zhang, X.-L.; Sun, H.-B. Nanostructures induced light harvesting enhancement in organic photovoltaics. *Nanophotonics* **2017**, *7* (2), 371–391. DOI: 10.1515/nanoph-2017-0060.
- (2) Carretero-Palacios, S.; Jiménez-Solano, A.; Míguez, H. Plasmonic Nanoparticles as Light-Harvesting Enhancers in Perovskite Solar Cells: A User's Guide. *ACS Energy Letters* **2016**, *1* (1), 323–331. DOI: 10.1021/acsenerylett.6b00138. Published Online: Jun. 17, 2016.
- (3) Naphade, R. A.; Tathavadekar, M.; Jog, J. P.; Agarkar, S.; Ogale, S. Plasmonic light harvesting of dye sensitized solar cells by Au-nanoparticle loaded TiO<sub>2</sub> nanofibers. *J. Mater. Chem. A* **2014**, *2* (4), 975–984. DOI: 10.1039/C3TA13246C.
- (4) Mascaretti, L.; Naldoni, A. Hot electron and thermal effects in plasmonic photocatalysis. *Journal of Applied Physics* **2020**, *128* (4), 41101. DOI: 10.1063/5.0013945.
- (5) Yu, Y.; Sundaresan, V.; Willets, K. A. Hot Carriers versus Thermal Effects: Resolving the Enhancement Mechanisms for Plasmon-Mediated Photoelectrochemical Reactions. *J. Phys. Chem. C* **2018**, *122* (9), 5040–5048. DOI: 10.1021/acs.jpcc.7b12080.
- (6) Gu, X.; Wang, H.; Camden, J. P. Utilizing light-triggered plasmon-driven catalysis reactions as a template for molecular delivery and release. *Chemical science* **2017**, *8* (9), 5902–5908. DOI: 10.1039/c7sc02089a. Published Online: Jun. 28, 2017.
- (7) Huynh, L. T. M.; Trinh, H. D.; Lee, S.; Yoon, S. Plasmon-driven protodeboronation reactions in nanogaps. *Nanoscale* **2020**, *12* (47), 24062–24069. DOI: 10.1039/d0nr07023h. Published Online: Nov. 27, 2020.

- (8) Brooks, J. L.; Warkentin, C. L.; Saha, D.; Keller, E. L.; Frontiera, R. R. Toward a mechanistic understanding of plasmon-mediated photocatalysis. *Nanophotonics* **2018**, *7* (11), 1697–1724. DOI: 10.1515/nanoph-2018-0073.
- (9) Zhang, Z.; Zhang, C.; Zheng, H.; Xu, H. Plasmon-Driven Catalysis on Molecules and Nanomaterials. *Accounts of chemical research* **2019**, *52* (9), 2506–2515. DOI: 10.1021/acs.accounts.9b00224. Published Online: Aug. 19, 2019.
- (10) Cho, F.-H.; Kuo, S.-C.; Lai, Y.-H. Surface-plasmon-induced azo coupling reaction between nitro compounds on dendritic silver monitored by surface-enhanced Raman spectroscopy. *RSC Adv.* **2017**, *7* (17), 10259–10265. DOI: 10.1039/C7RA00374A.
- (11) Sarhan, R. M.; Koopman, W.; Schuetz, R.; Schmid, T.; Liebig, F.; Koetz, J.; Bargheer, M. The importance of plasmonic heating for the plasmon-driven photodimerization of 4-nitrothiophenol. *Scientific reports* **2019**, *9* (1), 3060. DOI: 10.1038/s41598-019-38627-2. Published Online: Feb. 28, 2019.
- (12) Sheng, S.; Ji, Y.; Yan, X.; Wei, H.; Luo, Y.; Xu, H. Azo-Dimerization Mechanisms of p -Aminothiophenol and p -Nitrothiophenol Molecules on Plasmonic Metal Surfaces Revealed by Tip-/Surface-Enhanced Raman Spectroscopy. *J. Phys. Chem. C* **2020**, *124* (21), 11586–11594. DOI: 10.1021/acs.jpcc.0c01367.
- (13) Koopman, W.; Sarhan, R. M.; Stete, F.; Schmitt, C. N. Z.; Bargheer, M. Decoding the kinetic limitations of plasmon catalysis: the case of 4-nitrothiophenol dimerization. *Nanoscale* **2020**, *12* (48), 24411–24418. DOI: 10.1039/d0nr06039a.
- (14) Xu, P.; Kang, L.; Mack, N. H.; Schanze, K. S.; Han, X.; Wang, H.-L. Mechanistic understanding of surface plasmon assisted catalysis on a single particle: cyclic redox of 4-aminothiophenol. *Scientific reports* **2013**, *3*, 2997. DOI: 10.1038/srep02997. Published Online: Oct. 21, 2013.
- (15) Schürmann, R.; Ebel, K.; Nicolas, C.; Milosavljević, A. R.; Bald, I. Role of Valence Band States and Plasmonic Enhancement in Electron-Transfer-Induced Transformation of Nitrothiophenol. *J. Phys. Chem. Lett.* **2019**, *10* (11), 3153–3158. DOI: 10.1021/acs.jpcllett.9b00848. Published Online: May. 28, 2019.
- (16) Liu, P.; Wang, H.; Li, X.; Rui, M.; Zeng, H. Localized surface plasmon resonance of Cu nanoparticles by laser ablation in liquid media. *RSC Adv.* **2015**, *5* (97), 79738–79745. DOI: 10.1039/C5RA14933A.
- (17) Chan, G. H.; Zhao, J.; Hicks, E. M.; Schatz, G. C.; van Duyne, R. P. Plasmonic Properties of Copper Nanoparticles Fabricated by Nanosphere Lithography. *Nano Lett.* **2007**, *7* (7), 1947–1952. DOI: 10.1021/nl070648a.
- (18) Sotiriou, G. A.; Etterlin, G. D.; Spyrogianni, A.; Krumeich, F.; Leroux, J.-C.; Pratsinis, S. E. Plasmonic biocompatible silver-gold alloyed nanoparticles. *Chemical communications (Cambridge, England)* **2014**, *50* (88), 13559–13562. DOI: 10.1039/c4cc05297h.
- (19) Liu, D.; Zhou, F.; Li, C.; Zhang, T.; Zhang, H.; Cai, W.; Li, Y. Black Gold: Plasmonic Colloidosomes with Broadband Absorption Self-Assembled from Monodispersed Gold

Nanospheres by Using a Reverse Emulsion System. *Angewandte Chemie (International ed. in English)* **2015**, *54* (33), 9596–9600. DOI: 10.1002/anie.201503384. Published Online: Jun. 25, 2015.

(20) Ng, C.; Yap, L. W.; Roberts, A.; Cheng, W.; Gómez, D. E. Black Gold: Broadband, High Absorption of Visible Light for Photochemical Systems. *Adv. Funct. Mater.* **2017**, *27* (2), 1604080. DOI: 10.1002/adfm.201604080.

(21) Søndergaard, T.; Novikov, S. M.; Holmgaard, T.; Eriksen, R. L.; Beermann, J.; Han, Z.; Pedersen, K.; Bozhevolnyi, S. I. Plasmonic black gold by adiabatic nanofocusing and absorption of light in ultra-sharp convex grooves. *Nature communications* **2012**, *3*, 969. DOI: 10.1038/ncomms1976. Published Online: Jul. 24, 2012.

(22) Jain, P. K.; Lee, K. S.; El-Sayed, I. H.; El-Sayed, M. A. Calculated absorption and scattering properties of gold nanoparticles of different size, shape, and composition: applications in biological imaging and biomedicine. *The journal of physical chemistry. B* **2006**, *110* (14), 7238–7248. DOI: 10.1021/jp057170o.

(23) Dhiman, M.; Maity, A.; Das, A.; Belgamwar, R.; Chalke, B.; Lee, Y.; Sim, K.; Nam, J.-M.; Polshettiwar, V. Plasmonic colloidosomes of black gold for solar energy harvesting and hotspots directed catalysis for CO<sub>2</sub> to fuel conversion. *Chemical science* **2019**, *10* (27), 6594–6603. DOI: 10.1039/c9sc02369k. Published Online: Jul. 3, 2019.

(24) Kwon, N.; Oh, H.; Kim, R.; Sinha, A.; Kim, J.; Shin, J.; Chon, J. W. M.; Lim, B. Direct Chemical Synthesis of Plasmonic Black Colloidal Gold Superparticles with Broadband Absorption Properties. *Nano letters* **2018**, *18* (9), 5927–5932. DOI: 10.1021/acs.nanolett.8b02629. Published Online: Aug. 8, 2018.

(25) Yu, R.; Wang, J.; Han, M.; Zhang, M.; Zeng, P.; Dang, W.; Liu, J.; Yang, Z.; Hu, J.; Tian, Z. Overcurrent Electrodeposition of Fractal Plasmonic Black Gold with Broad-Band Absorption Properties for Excitation-Immune SERS. *ACS omega* **2020**, *5* (14), 8293–8298. DOI: 10.1021/acsomega.0c00698. Published Online: Apr. 2, 2020.

(26) Koopman, W.; Titov, E.; Sarhan, R. M.; Gaebel, T.; Schürmann, R.; Mostafa, A.; Kogikoski, S.; Milosavljević, A. R.; Stete, F.; Liebig, F.; Schmitt, C. N.; Koetz, J.; Bald, I.; Saalfrank, P.; Bargheer, M. The Role of Structural Flexibility in Plasmon-Driven Coupling Reactions: Kinetic Limitations in the Dimerization of Nitro-Benzenes. *Adv. Mater. Interfaces* **2021**, *8* (22), 2101344. DOI: 10.1002/admi.202101344.

(27) Schmidt, B.; Wolf, F.; Brunner, H. Styrylsulfonates and -Sulfonamides through Pd-Catalysed Matsuda-Heck Reactions of Vinylsulfonic Acid Derivatives and Arenediazonium Salts. *Eur. J. Org. Chem.* **2016**, *2016* (17), 2972–2982. DOI: 10.1002/ejoc.201600469.

(28) Zhao, Y.; Opitz, A.; Eljarrat, A.; Kochovski, Z.; Koch, C. T.; Koch, N.; Lu, Y. Kinetic Study on the Adsorption of 2,3,5,6-Tetrafluoro-7,7,8,8-tetracyanoquinodimethane on Ag Nanoparticles in Chloroform: Implications for the Charge Transfer Complex of Ag–F<sub>4</sub>TCNQ. *ACS Appl. Nano Mater.* **2021**, *4* (11), 11625–11635. DOI: 10.1021/acsanm.1c02153.

- (29) Dong, J.; Carpinone, P. L.; Pyrgiotakis, G.; Demokritou, P.; Moudgil, B. M. Synthesis of Precision Gold Nanoparticles Using Turkevich Method. *Kona : powder science and technology in Japan* **2020**, *37*, 224–232. DOI: 10.14356/kona.2020011. Published Online: Feb. 29, 2020.
- (30) Kimling, J.; Maier, M.; Okenve, B.; Kotaidis, V.; Ballot, H.; Plech, A. Turkevich method for gold nanoparticle synthesis revisited. *The journal of physical chemistry. B* **2006**, *110* (32), 15700–15707. DOI: 10.1021/jp061667w.
- (31) Gruenke, N. L.; Cardinal, M. F.; McAnally, M. O.; Frontiera, R. R.; Schatz, G. C.; van Duyne, R. P. Ultrafast and nonlinear surface-enhanced Raman spectroscopy. *Chemical Society reviews* **2016**, *45* (8), 2263–2290. DOI: 10.1039/c5cs00763a. Published Online: Feb. 5, 2016.
- (32) Yu, Y.; Wijesekara, K. D.; Xi, X.; Willets, K. A. Quantifying Wavelength-Dependent Plasmonic Hot Carrier Energy Distributions at Metal/Semiconductor Interfaces. *ACS nano* **2019**, *13* (3), 3629–3637. DOI: 10.1021/acsnano.9b00219. Published Online: Mar. 1, 2019.
- (33) Kang, L.; Xu, P.; Zhang, B.; Tsai, H.; Han, X.; Wang, H.-L. Laser wavelength- and power-dependent plasmon-driven chemical reactions monitored using single particle surface enhanced Raman spectroscopy. *Chemical communications (Cambridge, England)* **2013**, *49* (33), 3389–3391. DOI: 10.1039/c3cc40732b.
- (34) Feng, H.; Yang, Y.; You, Y.; Li, G.; Guo, J.; Yu, T.; Shen, Z.; Wu, T.; Xing, B. Simple and rapid synthesis of ultrathin gold nanowires, their self-assembly and application in surface-enhanced Raman scattering. *Chemical communications (Cambridge, England)* **2009** (15), 1984–1986. DOI: 10.1039/b822507a. Published Online: Feb. 23, 2009.
- (35) Polte, J.; Ahner, T. T.; Delissen, F.; Sokolov, S.; Emmerling, F.; Thünemann, A. F.; Kraehnert, R. Mechanism of gold nanoparticle formation in the classical citrate synthesis method derived from coupled in situ XANES and SAXS evaluation. *Journal of the American Chemical Society* **2010**, *132* (4), 1296–1301. DOI: 10.1021/ja906506j.
- (36) Kim, M.; Lee, J.-H.; Nam, J.-M. Plasmonic Photothermal Nanoparticles for Biomedical Applications. *Advanced science (Weinheim, Baden-Wuerttemberg, Germany)* **2019**, *6* (17), 1900471. DOI: 10.1002/advs.201900471. Published Online: Jul. 22, 2019.
- (37) Ahn, W.; Roper, D. K. Transformed Gold Island Film Improves Light-to-Heat Transduction of Nanoparticles on Silica Capillaries. *J. Phys. Chem. C* **2008**, *112* (32), 12214–12218. DOI: 10.1021/jp802497v.
- (38) Li, B.; Wang, Q.; Zou, R.; Liu, X.; Xu, K.; Li, W.; Hu, J. Cu<sub>7</sub>.2S<sub>4</sub> nanocrystals: a novel photothermal agent with a 56.7% photothermal conversion efficiency for photothermal therapy of cancer cells. *Nanoscale* **2014**, *6* (6), 3274–3282. DOI: 10.1039/c3nr06242b. Published Online: Feb. 7, 2014.
- (39) Liu, X.; Li, B.; Fu, F.; Xu, K.; Zou, R.; Wang, Q.; Zhang, B.; Chen, Z.; Hu, J. Facile synthesis of biocompatible cysteine-coated CuS nanoparticles with high photothermal conversion efficiency for cancer therapy. *Dalton transactions (Cambridge, England : 2003)* **2014**, *43* (30), 11709–11715. DOI: 10.1039/c4dt00424h. Published Online: Jun. 20, 2014.

- (40) Liebig, F.; Sarhan, R. M.; Sander, M.; Koopman, W.; Schuetz, R.; Bargheer, M.; Koetz, J. Deposition of Gold Nanotriangles in Large Scale Close-Packed Monolayers for X-ray-Based Temperature Calibration and SERS Monitoring of Plasmon-Driven Catalytic Reactions. *ACS applied materials & interfaces* **2017**, *9* (23), 20247–20253. DOI: 10.1021/acsami.7b07231. Published Online: May. 31, 2017.
- (41) Mo, F.; Di Qiu; Zhang, L.; Wang, J. Recent Development of Aryl Diazonium Chemistry for the Derivatization of Aromatic Compounds. *Chemical reviews* **2021**, *121* (10), 5741–5829. DOI: 10.1021/acs.chemrev.0c01030. Published Online: Apr. 9, 2021.
- (42) Nguyen, V.-Q.; Ai, Y.; Martin, P.; Lacroix, J.-C. Plasmon-Induced Nanolocalized Reduction of Diazonium Salts. *ACS omega* **2017**, *2* (5), 1947–1955. DOI: 10.1021/acsomega.7b00394. Published Online: May. 10, 2017.
- (43) Betelu, S.; Tijunelyte, I.; Boubekur-Lecaque, L.; Ignatiadis, I.; Ibrahim, J.; Gaboreau, S.; Berho, C.; Toury, T.; Guenin, E.; Lidgi-Guigui, N.; Félidj, N.; Rinnert, E.; La Chapelle, M. L. d. Evidence of the Grafting Mechanisms of Diazonium Salts on Gold Nanostructures. *J. Phys. Chem. C* **2016**, *120* (32), 18158–18166. DOI: 10.1021/acs.jpcc.6b06486.
- (44) Szczerbiński, J.; Gyr, L.; Kaeslin, J.; Zenobi, R. Plasmon-Driven Photocatalysis Leads to Products Known from E-beam and X-ray-Induced Surface Chemistry. *Nano Lett.* **2018**, *18* (11), 6740–6749. DOI: 10.1021/acs.nanolett.8b02426. Published Online: Oct. 8, 2018.
- (45) Heck, C.; Kanehira, Y.; Kneipp, J.; Bald, I. Amorphous Carbon Generation as a Photocatalytic Reaction on DNA-Assembled Gold and Silver Nanostructures. *Molecules (Basel, Switzerland)* **2019**, *24* (12). DOI: 10.3390/molecules24122324. Published Online: Jun. 24, 2019.
- (46) Kogikoski, S.; Dutta, A.; Bald, I. Spatial Separation of Plasmonic Hot-Electron Generation and a Hydrodehalogenation Reaction Center Using a DNA Wire. *ACS nano* **2021**, *15* (12), 20562–20573. DOI: 10.1021/acsnano.1c09176. Published Online: Dec. 7, 2021.
- (47) Dutta, A.; Schürmann, R.; Kogikoski, S.; Mueller, N. S.; Reich, S.; Bald, I. Kinetics and Mechanism of Plasmon-Driven Dehalogenation Reaction of Brominated Purine Nucleobases on Ag and Au. *ACS catalysis* **2021**, *11* (13), 8370–8381. DOI: 10.1021/acscatal.1c01851. Published Online: Jun. 23, 2021.
- (48) Schürmann, R.; Nagel, A.; Juergensen, S.; Pathak, A.; Reich, S.; Pacholski, C.; Bald, I. Microscopic Understanding of Reaction Rates Observed in Plasmon Chemistry of Nanoparticle–Ligand Systems. *J. Phys. Chem. C* **2022**, *126* (11), 5333–5342. DOI: 10.1021/acs.jpcc.2c00278.
- (49) Le Chang; Besteiro, L. V.; Sun, J.; Santiago, E. Y.; Gray, S. K.; Wang, Z.; Govorov, A. O. Electronic Structure of the Plasmons in Metal Nanocrystals: Fundamental Limitations for the Energy Efficiency of Hot Electron Generation. *ACS Energy Lett.* **2019**, *4* (10), 2552–2568. DOI: 10.1021/acsenergylett.9b01617.

TOC

